DOI: 10.1002/ejic.200501145

Carbon and Polymer Filaments in Nanoporous Alumina

Jörg J. Schneider*[a] and Jörg Engstler[a]

Keywords: Alumina / Porous templates / Nanotubes / Carbon / Nanochemistry

Nanoporous alumina membranes represent templates for the synthesis and alignment of filamentous nanostructured materials. Porous aluminium oxide (PAOX) membranes are ideal for high-temperature synthesis. They are transparent, flexible, freestanding and thermally robust. Their pore sizes can be varied over a wide range. The membrane backside seems suited for structuring processes on the nanoscale, for which it may serve as a master. After introducing the formation process of PAOX membranes, synthesis of carbon nanotubes (CNTs) with different morphologies, their electrical field emission properties, and the formation of polymeric filaments and structured polymer surfaces with the aid of PAOX are reported in this microreview.

1. Introduction

Nanotubes derived from various carbon sources, doped with non-carbon atoms[1] or pure inorganic tubes[2] such as MoS_2,[3] WS_2,[4] BN,[5] are intensively studied over the last years because of their unique material properties. Besides the challenge towards the synthesis of such materials, there is also the need to arrange such materials in an organized manner. One important research goal is to synthesize and organize nanomaterials in a single process step that allows for their 1D, 2D, or even 3D arrangement. A common and widely used technique for 2D structuring of nanomaterials is the template process, in which a given form acts as a structure-directing shape to organize individual building blocks in a 2D arrangement. Inorganic templates are typically solid phases; they can be crystalline or amorphous. They are stable with respect to a geometrically defined structure and usually up to higher temperatures. Zeolites are prominent examples of such template types. They enable the organization of matter in a 1D or 3D fashion. Unordered inorganic porous structures bearing multiple voids

[a] Fachbereich Chemie, Eduard-Zintl-Institut für Anorganische und Physikalische Chemie, Technische Universität Darmstadt, Petersenstraße 18, 64287 Darmstadt, Germany
Fax: +49-6151-16-3470
E-Mail: joerg.schneider@ac.chemie.tu-darmstadt.de

Jörg J. Schneider obtained his diploma and doctoral degree in chemistry at the Philipps-Universität Marburg in 1986, both in the group of Ch. Elschenbroich. After a one-year post doctoral stay in the group of K. J. Klabunde, USA, he joined the Max-Planck-Institut für Kohlenforschung, Mülheim an der Ruhr, in 1988. In 1994 he moved to the University of Essen as lecturer and Heisenberg fellow of the Deutsche Forschungsgemeinschaft. In 2000 he accepted a call as professor of inorganic chemistry at the Karl-Franzens-Universität, Graz, Austria. In 2003 he moved to his current position as professor of inorganic chemistry at the University of Technology, Darmstadt. His research interests are currently oriented towards interdisciplinary aspects of materials synthesis as well as organometallic chemistry. Examples include synthesis and properties of carbon tubes, porous materials, multinuclear metal complexes of condensed aromatics, as well as metal vapour synthesis as a synthetic tool in organometallic and materials chemistry.

Jörg Engstler was born in 1973. He studied chemistry at the University of Essen, Germany and obtained his diploma degree in 2000 in the field of synthesis and arrangement of carbon nanotubes. In the same year he moved to the Karl-Franzens-Universität, Graz, Austria, for pursuing his Ph.D. studies in the group of J. J. Schneider. His research activity was focussed on the synthesis and enhancement of field-emission properties of carbon nanotubes in and on porous alumina. In 2003 he received a Dr. rer nat. from the University of Essen. Since 2003, he is a post doc in the group of J. J. Schneider at TU Darmstadt, Germany. His research interests are in the area of porous nanomaterials, CVD and microscopic characterization techniques.

MICROREVIEWS: This feature introduces the readers to the authors' research through a concise overview of the selected topic. Reference to important work from others in the field is included.

and pores of nonuniform diameters that are randomly distributed in the material are another kind of such a template. Those materials can typically not be used for the controlled organization of matter in 2D or 3D dimensions, because their pores appear unordered.

For creating filamentous nanomaterials with functional properties, for example for optics or electronics applications, a defined 1D orientation of materials and therefore of the pore structure of the template is essential. Zeolite-based templates like MCM 41, as well as organic-based templates, for example polycarbonate membranes, are useful in this regard. However, membrane templates based on organic materials are often temperature-sensitive, and therefore high-temperature processes within the membranes often employed for the synthesis of inorganic nanostructures are impossible with these templates.

Anodic porous aluminium oxide (PAOX) is a valuable template material for high-temperature processes. It is widely used in the scientific community as a template for synthesis and organization of nanomaterials.[6] Recently Schmid has reviewed the synthesis and properties of various nanoparticle compositions in PAOX.[7] Synthesis, arrangement and properties of different rod-shaped magnetic materials in PAOX have been reviewed by Wade.[8] Our contribution presented herein is focussed on the generation, properties and 2D arrangement of CNTs and filamentous polymeric structures, both made by gas-phase processes in and on the surface of PAOX.

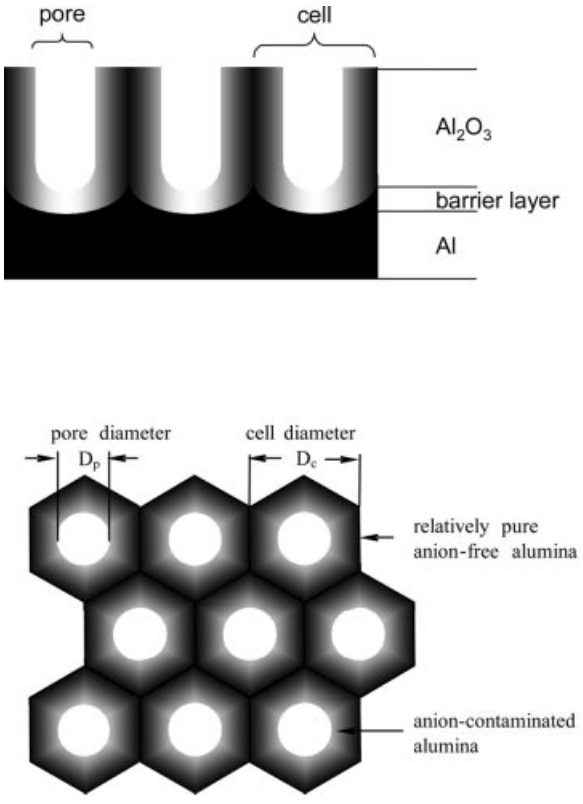

Figure 1. Schematic drawing of PAOX with idealized hexagonal ordered cells (diameter D_c) with a pore (diameter D_p) in the centre of each cell; cross-section (top), view from the top of the pore arrangement (bottom).

2. Nanoporous Anodic Aluminium Oxide as Template for Nanofilament Arrangement

The process of electrolytic oxidation of aluminium has a long-standing technological relevance and is commercially used for surface processing of aluminium for many decades. The pore system of alumina is formed by potentiostatic anodization, which is characterized by a constant voltage with a current change due to increased resistance in the growing oxide. The morphology of PAOX films synthesized in sulfuric acid has been investigated by Keller et al. already in 1953.[9] Early studies on the growth mechanism were performed by O'Sullivan and Wood in 1970.[10]

Formation and Structure of PAOX

Figure 1 shows a schematic drawing of a PAOX membrane with a hexagonally ordered pore system.

The membrane consists of hexagonally ordered cells with one centred pore in each cell. Each cell has a unidirectional shape orthogonal to the membrane surface. The bottom of the pores is sealed by the so-called barrier layer, which connects the PAOX membrane with the aluminium metal base from which the porous membrane grows in a self-organized manner during an ongoing electrochemical oxidation process. This barrier layer is compact, however it has numerous defects due to the permanent dissolution by the electrolyte. These defects (channels, pits, voids) are the starting points for regular pore formation in latter stages of the electrochemical oxidation. Thus redissolving alumina and ongoing aluminium oxidation are competitive processes (see below). The finally resulting highly ordered PAOX membrane has a porosity of up to 10% with pore densities of up to 10^{11} pores per cm^2.[11] When a disordered growth is observed, the overall porosity can be significantly lower or higher.[12] The pore walls of the cells consist of two different types of alumina.[12] One type is a relatively pure, anion-free, dense alumina (dark grey regions in Figure 1, bottom). It builds up the hexagonal body of the cell. This material is not in direct contact with the open pore space. The inner cell region of the pores consists of a less dense alumina (light grey regions in Figure 1, bottom) contaminated with electrolyte anions (PO_4^{3-} SO_4^{2-}, $C_2O_4^{2-}$), which forms the pore wall and therefore is in direct contact with the electrolyte during the electrochemical process. By controlled selective etching of the backside barrier layer, PAOX membranes with complete trough-hole pore morphology can be obtained.

The diameter of the pores (D_p) and the cells (D_c) of a PAOX membrane are dependent on the anodization potential applied in the electrolytic process.[6h,13] Additional experimental parameters governing the pore size are temperature and current density. The latter is influenced by the concentration and the type of electrolyte used.[11]

PAOX membrane pore diameters between ca. 5–300 nm are so far experimentally accessible. As a rule of thumb, a voltage of 1 V corresponds to a pore growth of ca.

1.2 nm.[10] This value depends on anodization conditions and electrolyte concentration. Figure 2 shows examples of electron micrographs of PAOX membranes with varying pore diameters (Figure 2).

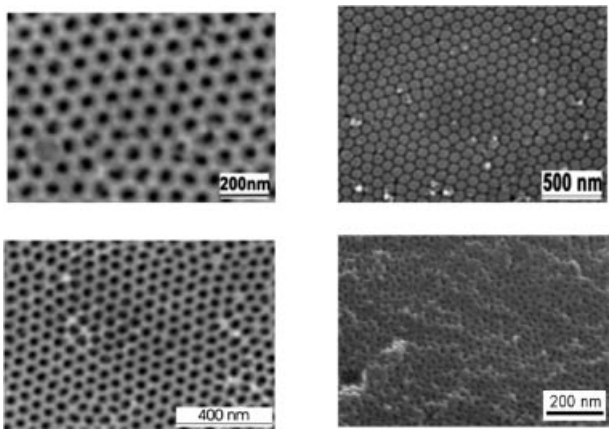

Figure 2. SEM images of freestanding PAOX membranes. From upper left to lower right: open front side of a PAOX membrane generated at 40 V, back side of a PAOX membrane generated at 40 V, open front side of a PAOX membrane generated at 25 V, open front side of a PAOX membrane generated at 8 V.

To obtain PAOX templates with different pore size regimes, different electrolytes are used. From 150 to 300 nm H_3PO_4, from 30 to 70 nm oxalic acid and below 20 nm H_2SO_4 give reproducible results with respect to pore-size diameters.[8] This electrolyte dependence of pore size distribution is mainly due to the fact that the pore diameter is affected strongly by the dissolution velocity of alumina in the electrolyte chosen. The dependence of pore size on electrolyte type is, however, complex and involves the dissociation behaviour (pH value, acid/conjugate base equilibrium) and concentration of the electrolyte (e.g. changing the electrolyte concentration changes the pH) as the foremost parameters.

The basic membrane-film-forming reaction is dissolution of the base metal according to

$$Al(s) \rightarrow Al^{3+} + 3e^-$$

Al_2O_3 is then formed by reaction with O^{2-} ions which are generated in the acidic electrolyte medium by the reaction

$$3/2\ H_2O \rightarrow 3\ H^+ + 3/2\ O^{2-}$$

The formation process of the alumina is accompanied by a local dissolution of the formed alumina due to agitation by protons

$$1/2\ Al_2O_3(s) + 3\ H^+(aq) \rightarrow Al^{3+}(aq) + 3/2\ H_2O(l)$$

The latter reaction preferentially occurs at the bottom of the formed pores where the electrical field is highest. This reaction obviously does not play an important role during the initial formation of the compact base oxide layer lying underneath the porous layer.

During electrolyte anion incorporation into the growing membrane, the following reactions occur:[6h]

$$H_3PO_4\ (aq) \rightarrow H_2PO_4^{2-} + H^+$$

$$H_2PO_4^-\ (aq) \rightarrow HPO_4^{2-} + H^+$$

The conjugate divalent base anion HPO_4^{2-} can replace O^{2-} in the oxide forming reaction, thus leading to a contamination in the growing film. Therefore 6–8 wt.-% PO_4^{3-} incorporation of the membranes is typically observed when phosphoric acid is used the electrolyte. Similar percentages of incorporation are observed for other electrolyte anions (SO_4^{2-}, $C_2O_4^{2-}$). In contrast, electrolytes which do not form protonated conjugate bases lead to contamination of free PAOX membranes (e.g. chromic acid[6h]).

The electrochemical process of controlling and downsizing the pore diameter by adjusting the anodization voltage as one of the crucial parameters works well down to pore sizes of around 15 nm in the strong electrolyte H_2SO_4. There is an interest in such nanoporous self-supporting template materials due to their application as nanovessels for synthesis and organization of matter on the nanoscale. In the size regime below 15 nm, quantum size effects start to become important for many materials, and a self-supporting porous template should make it possible to study anisotropic effects of such structure-confined materials. However, reports on self-supporting PAOX membranes with a pore size below ca. 15 nm are scarce. Highly unordered PAOX films deposited on glass substrates with small pore diameters (<10 nm) are known.[14–16] We have studied pore-size growth of PAOX at anodization voltages down to 8 V. Formation of a porous alumina with a pore diameter of about 10 nm results. Handling these PAOX membranes as freestanding templates, however, becomes increasingly difficult: for example, such membrane templates tend to be brittle and are mechanically fragile. In contrast, PAOX membranes with pore sizes between 20 and several 100 nm exhibit good mechanical stability. They are not very fragile and can withstand even moderate mechanical torsion, for example bending. The reason for this is their cellular structure. It is well known that if pores in a given cellular structure are hexagonally oriented, the mechanical stiffness of such a cellular arrangement decreases roughly by a factor of 50 compared to a similar compact structure.[17] This finding is based on the variation of the *E*-module which is dramatically affected when comparing a compact with a porous structure. In a first approximation, this is regardless of the individual material composition of such a structure.

Thus, the high tensile strength of the as-prepared PAOX template relative to a dense, compact alumina film of the same composition seems mainly due to its mechanical flexibility imparted by its regular open porous nature relative to the dense material of same composition.

3. Carbon Nanotubes and Polymer Fibres in PAOX

3.1 Carbon Nanotubes in PAOX

CNTs Synthesized in PAOX without Catalyst

Spatially arranged CNTs provide a promising material for applications in e.g. Li-ion batteries,[18] chemical filters,[19] capacitors,[20] cold field emitting sources[21] or tran-

sistors.[22] PAOX is ideally suited as a template for CNT synthesis by CVD, a process which typically operates above 700 °C.[23–25] The diameter of the CNTs formed inside the PAOX template pores during CVD should be the same as the PAOX pore diameter. Hence, a general feature of PAOX, its versatility to control the diameter of the CNTs, becomes apparent.

In a typical experiment, a gaseous precursor like propylene or acetylene transported by a carrier gas is decomposed within a hot-wall tube reactor in which the open membrane is inserted vertically in a flow-through geometry.[26] The pores of the membrane are then completely filled with CNTs during the CVD process. Figure 3 shows a SEM image of such a CNT/PAOX membrane composite.

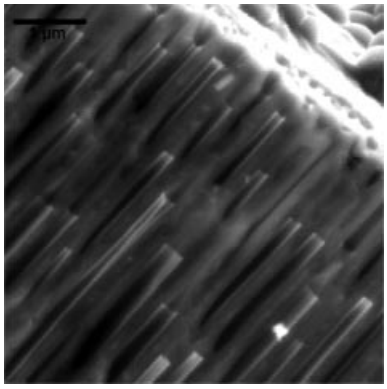

Figure 3. SEM image of a CNT/PAOX membrane composite showing a broken edge from which the CNTs protrude out of the pores of the PAOX.

Typical synthesis conditions for our CNT formation process are 900 °C, propylene flow between 1 mL and 14 mL per minute depending on the reaction time (5 min to 40 min). After the CVD process, the PAOX surface is usually covered with residual carbon materials. These can be "burned away" under controlled and mild oxidative conditions without destroying the CNTs.[26]

CNTs Synthesized in PAOX Loaded with Catalyst

PAOX templates can be loaded with appropriate catalyst precursors like inorganic Fe salts prior to CNT growth, for example simply by dip filling.[27,28] Under reducing conditions, flowing H_2 is used for this purpose; the active catalyst can then be generated in nanoparticle form.[29] The effect of the catalyst particles on CNT growth is twofold. On the one hand, the use of catalyst particles reduce the synthesis temperature for CNT growth, on the other hand, CNT graphitization can be achieved already at lower temperatures relative to an uncatalyzed CVD process.

Impregnation of PAOX membranes with a catalyst prior to CNT synthesis leads to a CNT/PAOX composite material. The CNT/PAOX composite material can be freed from the PAOX template by dissolving it in diluted HF. The resulting carbon filaments have a fibre-like compact structure as revealed by transmission electron microscopy (TEM). At a higher magnification, a tube-in-tube morphology ("carbon nanotube bags") can be identified by TEM (Figure 4).[29,30] The smaller inner tubes display helicoidal structures and are almost densely packed within the outer "carbon nanotube bags". The compact fibre-like material therefore contains two different carbon tube morphologies of different size. The outer, larger tubes are produced by the deposition of carbonaceous precursor species derived from the molecular precursor gas source (e.g. propylene). These CNTs are formed on the inner walls of the PAOX membrane during the CVD process. Their diameter is determined by the pore dimensions of the template. In this process, the inner walls of the PAOX template are cast.

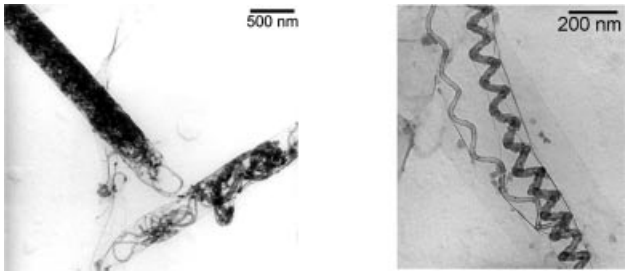

Figure 4. TEM image of "nanotube bags" freed from the PAOX template; left: the inner helicoidal CNTs are surrounded by the outer, larger CNT; right: helicoidal morphology of a single interior CNT.

The PAOX template pore walls represent a surface with high morphological roughness. This roughness is reflected in the morphology of the CNT walls, which show no ideal straight alignment but a rather high degree of dislocation of the carbon tube walls (Figure 5).

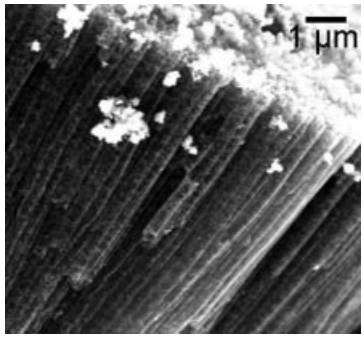

Figure 5. SEM micrograph showing PAOX-freed CNTs in typical parallel block arrangement.

The dense filling of the larger carbon tubes with the smaller helicoidal CNTs in their interior is due to a catalytic process. It is mediated by the iron particles which are derived from the catalyst precursor introduced into the PAOX by the impregnation step.[27] The diameter of the helicoidal inner CNTs is about 20 nm and corresponds well with the size of the catalyst particles which are mainly found at the end of the tubes (Figure 6).

In addition, TEM and AFM investigations[29] reveal that the diameter of the large outer CNTs is enlarged when freed from the template, relative to what is expected from the given size of the template pores in which they are formed. This fact can be understood by the only partially graphi-

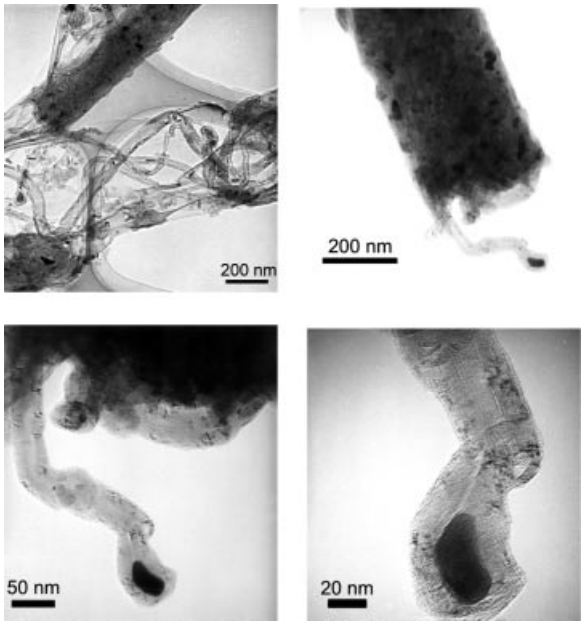

Figure 6. TEM images of CNT bags filled with small CNTs derived from catalyst impregnation. From upper left to lower right: overview of small CNTs with catalytic particles located at the end of the smaller inner tubes; different magnifications of CNT inner tubes with catalytic particles at the end of the small CNTs.

tized structure of the tube walls of the outer CNTs as it is revealed by high resolution TEM (HRTEM) investigations (Figure 7).

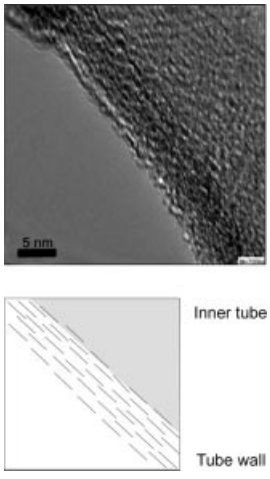

Figure 7. Top: HRTEM image of a "CNT bag" wall structure showing the partially graphitized wall structure; bottom: corresponding schematic model of the outer CNT wall structure.

The schematic model, which is in accord with the experimentally observed morphology found in the HRTEM, is shown in Figure 7. Relatively short multilayered, intermingled graphene sheets are characteristic for the CNT wall structure. This graphene sheet structure is flexible and allows the outer tubes to widen their diameter significantly when an inner pressure is exerted upon the walls. As long as the CNTs are embedded in the PAOX template, their diameter is fixed. However, when the CNTs are freed from the template, a dense filling of the CNTs may lead to a significant expansion of their diameter. This is a kind of "breathing process" which releases inner pressure from the CNT walls imposed on them by the dense filling with the small helicoidal tubes. Obviously, such a widening process can even lead to a rupture of the walls of the large CNTs and to the liberation of the entrapped small helicoidal tubes (Figure 8).

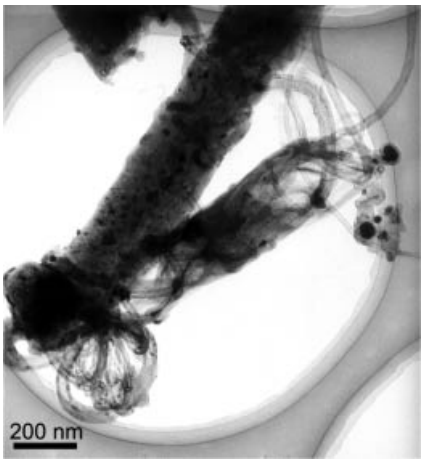

Figure 8. TEM of a compact CNT bag. After breaking the outer CNT wall, the inner CNTs swell out of their surrounding shell (bottom left).

We have studied the elastic properties of the carbon nanotube bags by AFM with the nanoindentation technique.[31–33] A Berkovitch-type indentation probe (100-nm

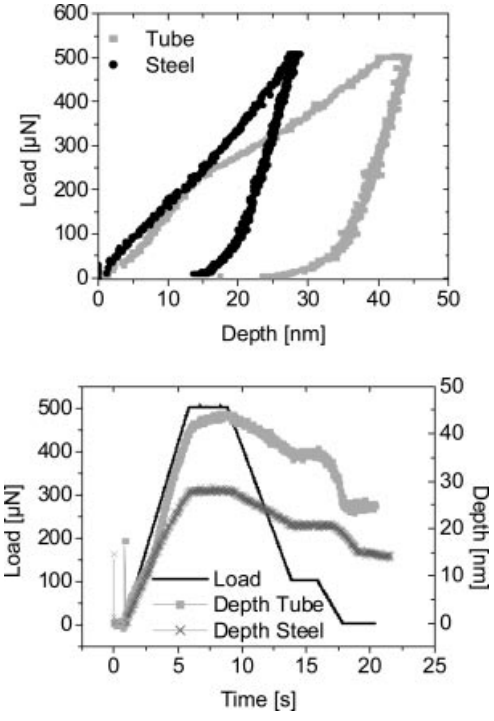

Figure 9. Nanoindentation loads (up to 500 μN) vs. indentation depth applied to a single filled carbon nanotube bag.

tip radius) was placed in the middle of a single carbon nanotube bag. Experiments were conducted with up to 500-μN loads on the tip (Figure 9, top). Up to loads of 220 μN, the indentation depth increased linearly with increasing load. In the low-load regime (up to ca. 60 μN) the CNT displayed viscoelastic behaviour with nearly no residual plastic deformation (<1 nm). When the final indentation load was increased to 500 μN, the depth of impression on the carbon nanotube bag structure increased considerably to 35 nm. However, at a load of 230 μN a sudden deviation from a linear behaviour was found (Figure 9, top).

After release of the maximum load a residual depth of impression of 27 nm remained in the material (Figure 9, bottom). Compared with the low-load regime, where a maximum load of 60 μN was applied, this dramatically different behaviour at higher loads may be attributed to a sudden rupture of the CNT wall structure. In the low-load regime, the filled CNT nanotubes show viscoelastic behaviour typically observed for soft matter (e.g. polymers), whereas high enough compression loads lead to the destruction of the outer CNTs (see Figure 8).

CNTs in PAOX Derived from Single-Source Precursor Molecules

There have been several reports on the synthesis of CNTs using single-source precursors.[34] Examples for such precursors are organometallic compounds like metallocenes or coordination compounds like iron(II)phthalocyanine.[35,36] In these precursors, there exists a fixed, stoichiometrically defined metal-to-carbon ratio. Ferrocene is a prominent precursor for CNT synthesis by CVD techniques.

Figure 10 displays a typical TEM image of CNTs derived from ferrocene as the sole CNT precursor. In these experiments, the CNTs have been first synthesized and then deposited freely on a freshly cleaved mica surface. Due to the low carbon-to-iron-catalyst ratio (10:1) when employing ferrocene, the CNTs are mostly filled with iron metal.[37]

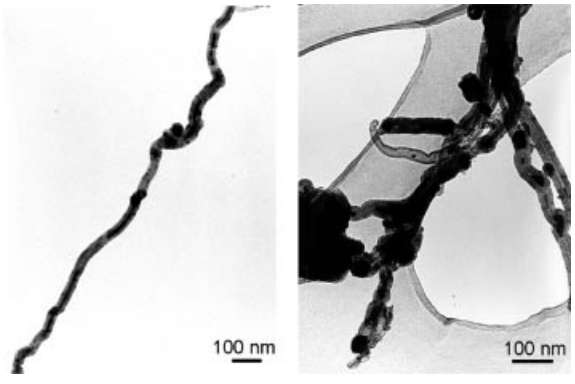

Figure 10. TEM images of CNTs synthesized via CVD of ferrocene on a native mica support at different magnifications.

When the carbon-to-iron ratio is increased by a factor of 7, CNTs with a much lower iron content are formed, and subsequently no formation of compact iron rods is observed inside the CNTs. Instead, particles are formed in the CNTs (Figure 11). An increase in the carbon-to-iron ratio was achieved by adding an additional carbon source to the ferrocene precursor.[38] We used the polycondensed aromatic hydrocarbon decacyclene $C_{36}H_{18}$ as the additional carbon source.[26,39,40]

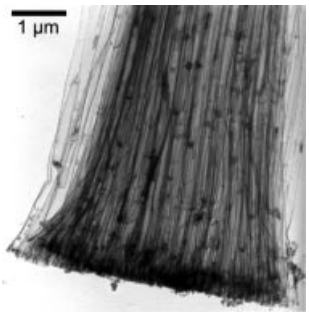

Figure 11. TEM micrograph of a CNT bundle synthesized by deposition of a mixture of decacyclene/ferrocene (70:1 at.-%) in PAOX (template removed).

Bundle-like arrangements of CNTs are found after dissolution of the PAOX template. Metal particles are distributed within these CNT bundles.

When using chromocene, $[(\eta^5\text{-}C_5H_5)_2Cr]$, a precursor with the same carbon-to-metal ratio as that in ferrocene, CNTs are formed under similar conditions (Figure 12). However, in contrast to the CNT material obtained from the ferrocene precursor, no metallic wires are formed within the tubes. The CNTs contain particles distributed alongside the CNTs, although the carbon-to-metal ratio is identical to that in ferrocene. Obviously, not only the stoichiometric carbon-to-metal ratio, but also the nature of the catalytic metal or the precursor are important for the filling of the CNTs, either with metallic rods or particles.

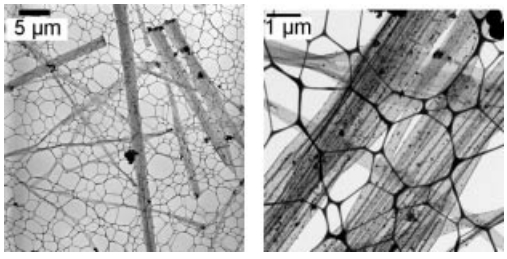

Figure 12. TEM micrographs of template-freed CNTs synthesized by deposition of chromocene in PAOX. A characteristic parallel-block arrangement of CNTs derived from PAOX is maintained (template removed).

Comparison of the results for CNT synthesis performed by the single-source strategy without a structure-directing template and those for the template-steered synthesis by using PAOX shows that the resulting CNT materials have different morphologies. CNTs prepared by the template technique display a parallel alignment of CNTs, with overall straight tube body morphology and defined tube radii. In contrast, CNTs prepared by a template-free CVD process by using a single-source strategy have a poorer straightness, a significant deviation in tube diameter and a random distribution of their metal filling.

Element-filtered TEM (EFTEM) has provided detailed information about the elemental distribution of CNT materials. In general, EFTEM enables the recording of two-dimensional distributions of chemical elements (Li to U) with a resolution down to about 1 nm. Chemical and structural heterogeneities may thus be imaged by recording elemental distributions. Applying this technique supplies an enormous amount of information relative to conventional bright-field TEM. In Figure 13, the results of such an EFTEM investigation of a single CNT synthesized by CVD by using chromocene as precursor and PAOX as template are shown.

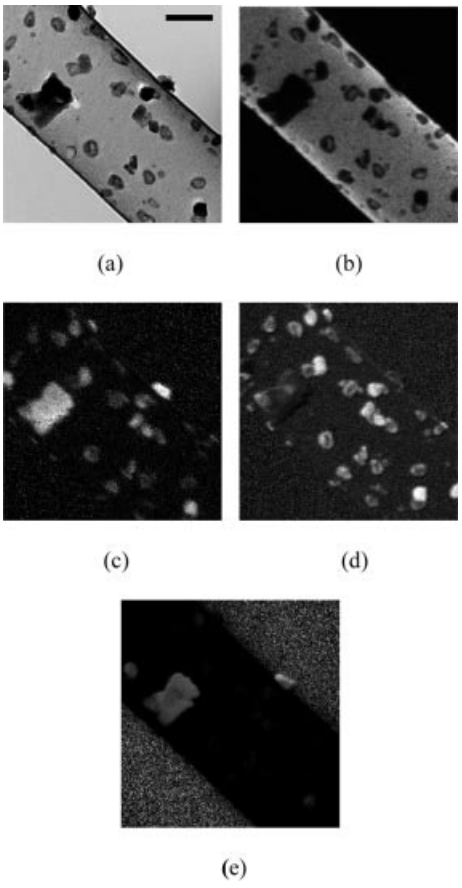

Figure 13. EFTEM investigations on a single CNT (precursor: chromocene): (a) bright-field image of a single CNT with incorporated particles; images of single-element distributions with elements displayed in lower contrast, (b) carbon, (c) oxygen, (d) chromium, (e) aluminium; (scalebar for all images: 100 nm).

The selective elemental mapping gives the spatial distribution along the CNT (Figure 13b–e). Obviously, chromium is a main constituent. Besides the elements chromium and carbon, oxygen is also present in the irregularly shaped particles, which have a diameter between 20 and 30 nm (shown in Figure 13c). Thus, the formation of chromium oxide particles seems reasonable. The formation of these oxide particles is yet unclear since the CVD process proceeds under otherwise inert conditions.

The origin of the detected alumina particles (Figure 13c,e: O and Al elemental maps) can be attributed to the incomplete dissolution process of the PAOX template during sample preparation, leaving minor amounts of residual alumina in the sample.

Similar experimental and EFTEM analytical results were obtained for the synthesis of CNTs by using metallocenes of Ni and Co as single-source precursors. In both cases, CNTs with diameters corresponding to the PAOX template were found. The CNTs again contained metal particles inside the tubes. Ultrathin samples of these CNTs, still embedded in the PAOX template, were studied by TEM (Figure 14).

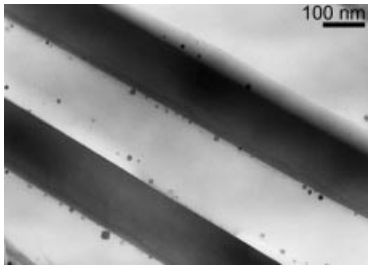

Figure 14. TEM image of an ultrathin sample of CNTs embedded in PAOX, obtained by microtoming (CVD precursor nickelocene). Dense regions which appear with a dark contrast display the PAOX template walls. Alongside the PAOX tube walls, small nickel particles are deposited. Some appear to be partly embedded in an amorphous carbon shell.

Particles with a high nickel content, which are found alongside the pore walls of the CNTs and/or the PAOX template, can be detected by EFTEM analysis of such samples. As for the chromocene case, oxygen is present, however its origin cannot be unambiguously determined, now because of the close proximity of the Ni particles to the surrounding alumina pore walls.

Field Emission from CNT Arrays

An interesting electrical property of CNTs is their field-emission (FE) behaviour. Because of their small diameter, the electronic working function of CNTs is dramatically reduced. Thus, a tunnelling effect of electrons can occur, and consequently theoretical and experimental studies on the electron emission of CNTs have been in the focus of research already for more than one decade.[39,41] Multiwalled CNTs (MWCNTs) are mechanically more robust and are also less prone to electrical degradation than single-walled CNTs (SWCNTs). The emission from MWCNTs shows metal-like behaviour, as deduced from electron spectroscopic studies.[42] For MWCNTs, characteristic parameters in FE, such as the onset field for emission, current density and electrical field enhancement factors β,[43] are drastically improved[44,45] relative to other relevant FE materials like diamond tips,[46] Si[47] and GaN,[48] which were studied intensively over the past years.

For isolated, single CNTs, ten times higher field enhancing factors β are observed relative to CNT films containing bundles of unordered tubes.[49] Thus, different strategies can be followed to obtain good field-emitting devices based on SWCNTs or MWCNTs. One general strategy seeks the most perfect two-dimensional arrangement of CNTs in order to

arrange as many emitters as possible on a substrate.[50] This assures that a huge number of high aspect ratio structures are produced and are available for FE. Another synthetic strategy arranges CNT emitters in defined areas with a high enough distance to each other, thus fulfilling the theoretical requirement that the distance between single emitters is about the height of an individual emitter to obtain long-term FE stability.[51] By realizing the latter approach, the inter-emitter field penetration due to charging and electrical degradation is significantly reduced relative to arrangements where a higher emitter density is achieved (Figure 15).

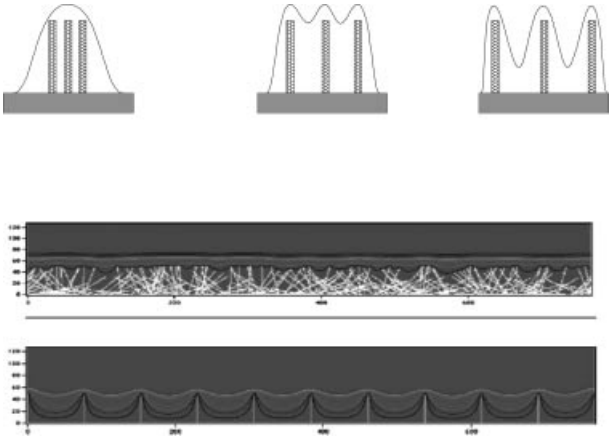

Figure 15. Schematics showing the dependence of the individual electrical field penetration of CNT emitters as a function of the emitter distance. Idealized model (top), model of a realistic CNT surface with high emitter surface coverage (bottom).

Densely populated CNT cathodes therefore have definite disadvantages in their FE behaviour at low fields due to mutual shielding effects (Figure 15).[51] Well-separated CNTs with still high enough densities per area and homogeneous FE characteristics, however, need synthesis techniques other than the former.[44] Up to this date, successful studies have been reported to optimize the FE performance for aligned CNTs.[41e,45,50,52–54] We used PAOX as a templating material for CNTs and investigated the resulting FE properties.[55] In these experiments, additional positive influences of PAOX on the FE behaviour could be detected: for example, electrical insulation of the CNT emitters due to their embedding in the dielectric matrix of PAOX seems advantageous in avoiding destructive degradation by field effects.[51] On the other hand, it has been observed that an outgrow of CNTs over the PAOX surface promotes FE properties.[56] For CNTs which are overgrowing the PAOX template structure, low onset fields for emission of 3–4 V μm^{-1} are found. In contrast to these results, CNTs which are totally embedded in PAOX and do not surmount the surface at all, have ten times higher onset fields for FE.[55]

Our work in the area of synthesis and arrangement of CNTs for FE applications has so far focussed on metallocenes or mixtures of metallocenes with polycondensed aromatics as precursors for CNT synthesis.[29,44,57–59] Growing of CNTs by using metallocene precursors was achieved in and on the surface of PAOX membranes and led to an unordered growth on the PAOX surface. Good FE characteristics for such materials were observed when alumina particles were first deposited by CVD from a precursor [source: aluminium tris(sec-butoxide)] on the PAOX surface prior to CNT deposition by CVD (precursor: ferrocene). Then, CNT growth preferentially occurred on the deposited alumina islands (Figure 16).[44,58–60]

FE measurements on this material where performed in a diode configuration. The emission picture was obtained after sample conditioning by current processing.[58,59] Sample conditioning is a standard procedure in FE studies and is necessary because the FE effect and especially the long-term stability of the emitters are very sensitive to any surface and gaseous atmospheric impurity.[58–60] Integral FE measurements on such samples have yielded current densities up to 32 mA cm^{-2} at 7.2 V μm^{-1}.[59] These values are based on a uniform emitter distribution and an emitter number density of 10000 cm^{-2}. This is so far a superior result compared with current values from other studies.[52–54]

Single-emitter investigations on the material revealed stable Fowler-Nordheim-like I–V curves.[58] Despite the observation of some short-term current fluctuations, the alumina-based CNT cathodes provide already reasonable long-term current stability (>18 h) as shown in Figure 17 and Figure 18.

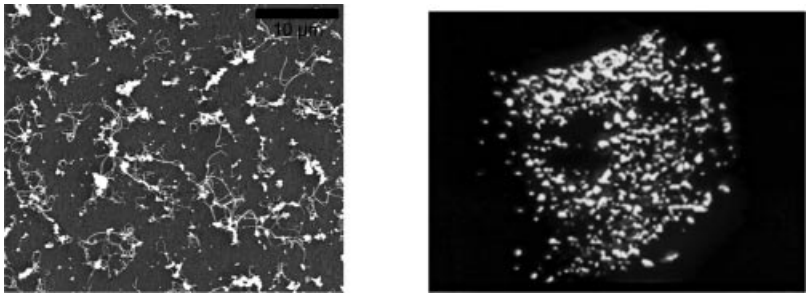

Figure 16. Typical SEM image of isolated CNTs grown on the surface of the PAOX membrane by CVD for FE investigations. The CNTs responsible for FE are linked to the surface of the PAOX by CVD deposition on predeposited alumina islands; right: emission picture of such a sample (size 28 mm^2) after conditioning (see text).[59]

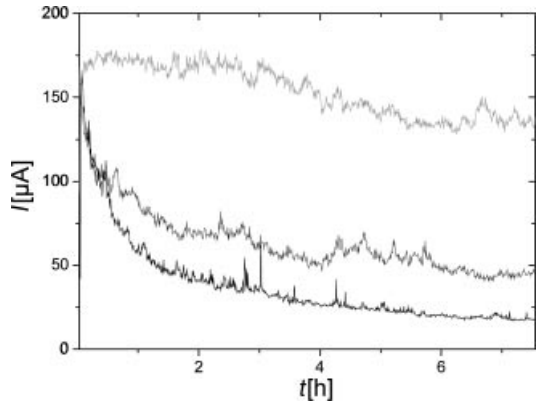

Figure 17. Long-term current stability of a 28-mm^2 sample on PAOX at various pressures/fields: 2×10^{-6} mbar at 4.6 V µm^{-1} (upper trace); 5×10^{-5} mbar at 5.3 V µm^{-1} (middle trace); 5×10^{-4} mbar at 6.5 V µm^{-1} (lower trace).[59]

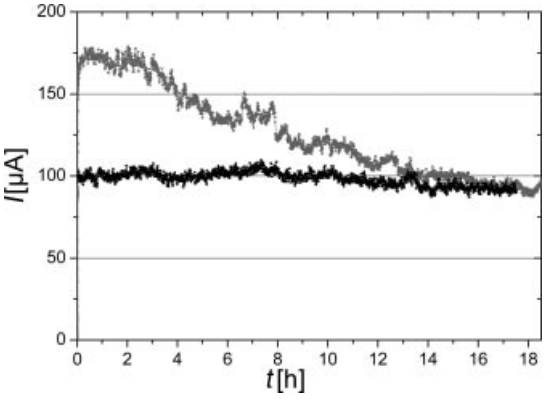

Figure 18. Comparison of the typical long-term current stability of a CNT cathode measured at 10^{-6} mbar at 4.6 V µm^{-1} before (upper trace) and after processing (lower trace) up to 700 µA.[59]

Nevertheless, developing stable CNT field emitters with high performance characteristics is an important task in this research area (long-term stability ≥ 10000 h). Furthermore, an aligned and directed growth of CNTs has to be realized in order to obtain well-separated nanotubes. Such an alignment of emitter structures is so far only realized in Spindt type configurations, which are up to now still the only industrially viable field emitter structures.

3.2 Polymeric Structures in and on PAOX

Synthesis and Alignment of Polymeric Poly(p-xylene) (PPX) Filaments Derived from PAOX

The first reports on the synthesis of polymer tubes and cylinders in PAOX templates appeared in the mid 1990s.[61–63] A recently explored technique uses the controlled wetting of ordered pores of PAOX to generate polymer nanotubes.[64,65] In this approach, the high-energy surface of a PAOX membrane is wetted by a low-energy organic polymer to fill the pores and mould the PAOX template structure. This results in formation of polymeric nanotubes after removal of the template. With this technique, 2D arranged polystyrene, polytetrafluoroethylene (PTFE), polymethyl methacrylate (PMMA) or palladium/polymer composite materials are accessible in filamentous form, either embedded in the template or freed from the template.[64,65] 2D confinement studies of symmetric and asymmetric block copolymers in PAOX templates have been reported recently.[66,67] Formation of polymer or block copolymer nanorods is driven by capillary forces which force the polymer[66] or copolymer melt[67] into the cylindrical nanopores of the PAOX template. These studies show that microphase separated copolymers are formed within the nanochannels of PAOX. The observed polymer structures are not only triggered by the pore size of the template but also by the specific interaction of pore wall with polymer, leading to phase-segregated copolymer rods in which for example styrene or polybutadiene forms the central core.[67,68]

Gas phase processes have been studied recently to form tube- or wire-like structures of other technically important polymers, like poly(*p*-xylene), PPX, in PAOX.[68] PPX films have very good electrical insulation and barrier properties, excellent solvent and hydrolytic resistance, biocompatibility, transparency and thermomechanical properties. PPX is formed by evaporation and vapour-phase pyrolysis of [2.2]-paracyclophanes as precursors. 1,4-Quinodimethanes are formed as intermediates, acting as monomers (Scheme 1). The in situ formed quinodimethanes polymerize spontaneously on nearly any given substrate upon vapour phase deposition at temperatures equal to or below 30 °C by formation of conformal highly adhesive PPX films.[69]

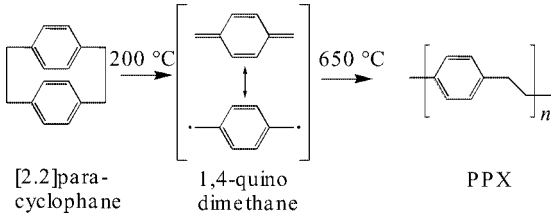

Scheme 1. Formation of PPX polymer starting from [2.2]paracyclophane precursor via intermediate 1,4-quinodimethane.

Within PAOX, PPX can be synthesized in a fibre morphology by chemical vapour deposition polymerization. Figure 19 shows a top and side view of a PPX film formed on PAOX after CVD polymerization deposition. PPX forms a closed film on top of the template, covering its surface completely.

PPX fibres are formed within the pores of the template (Figure 19). The compact PPX films on top of the template can be detached from the surface mechanically or by chemical techniques.

The ordered backside of PAOX membranes can be used for patterning a polymer such as PPX in a straightforward technique by moulding the backside when using it as a master form. This master backside with desired nanodimensions can be prepared by electrochemical oxidation of aluminium metal and detachment of the film from the metal base. This simple technique avoids complicated physical structuring processes like e-beam lithography for shaping a

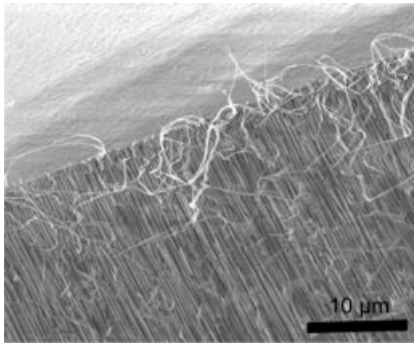

Figure 19. SEM image of a PAOX/PPX composite surface. Fibrous PPX structures protude out of the pores of the PAOX template.

master form, which can then be used in the moulding process. Instead, the self-organization process of forming the nanostructured alumina cells is used to produce the master form. The barrier layer of PAOX provides a nanostructured surface with regular hexagonally ordered concave domes (Figure 20). A replication of the backside PAOX structure with a polymer film may thus represent a straightforward way to nanostructured polymer surfaces with an inverse morphology when detached from the master.

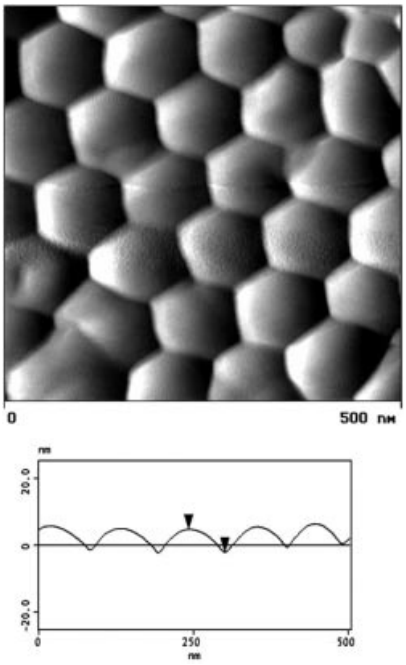

Figure 20. AFM image of a closed PAOX backside with hexagonal pore order used as master in moulding experiments with PPX; bottom: corresponding height profile.

The coating of the PAOX backside template with a thin PPX film can be done in a CVD reactor consisting of a quartz reactor tube in which a three-zone heating can be realized. A temperature gradient from 170° to 700 °C is suitable for sublimation and for initiating the in situ CVD polymerization. After CVD polymerization, the PPX film on the backside of the membrane can either be lifted off mechanically or detached chemically from the resulting PPX/PAOX composite to give a structured PPX film. This process is shown schematically in Figure 21.

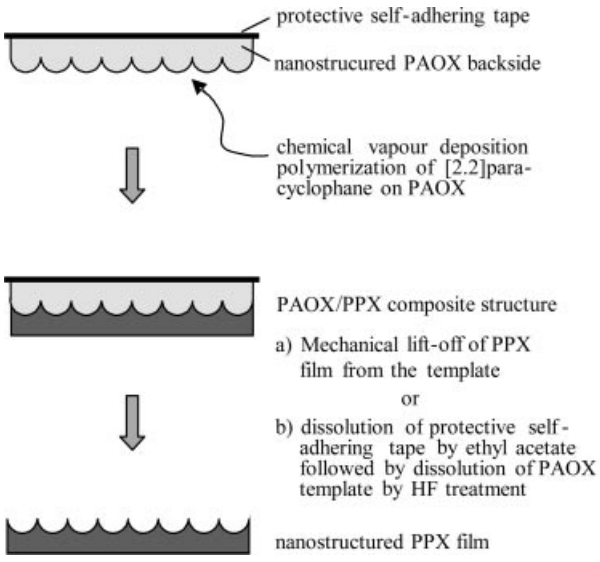

Figure 21. Schematic drawing showing the steps involved in the moulding of a PAOX backside to yield a PPX polymer as well as its detachment to obtain a freestanding nanostructured PPX film.

Figure 22 compares the appearance of a structured PPX film after mechanical lift-off with that after chemical detachment from the PAOX template. The breaking of the film by mechanical stress during the detachment results in the formation of fibrous structures. In contrast, the morphology of the structured PPX film can be retained intact over wide areas by chemical detachment from the master. The film then shows a regular concave structure, in which the small dimples mirror an almost ideal replication of the convex dome-like PAOX backside structure.

Such nanostructured surfaces may show a drastically altered wetting behaviour. Measuring the contact angle at a solid/liquid/gas interface is a very sensitive surface analytical method. It probes the outer atomic layers of a surface and enables the study of chemical as well as morphological surface changes.[70,71]

The hydrophilicity/hydrophobicity of a surface can be determined by measuring the contact angle Θ between water and the surface (Figure 23). A contact angle of 0° relates to a flat monomolecular water film on a surface of a solid. At a contact angle of 180°, a drop of water, for example, is in contact with the surface only at a single point (superhydrophobic). Between these extremes, surfaces are termed hydrophilic (<90°) or hydrophobic (>90°).

The contact angle of water on a flat PPX surface is 86° (weak hydrophilic behaviour). This compares with an angle of 14° for water on a flat glass surface (roughness ≤ 0.5 nm, piranha-solution-cleaned glass), which is classified as superhydrophilic.[72] The nanostructured PPX film (see Figure 22) which represents a rough surface, shows a drastically reduced water contact angle of only 24° compared to

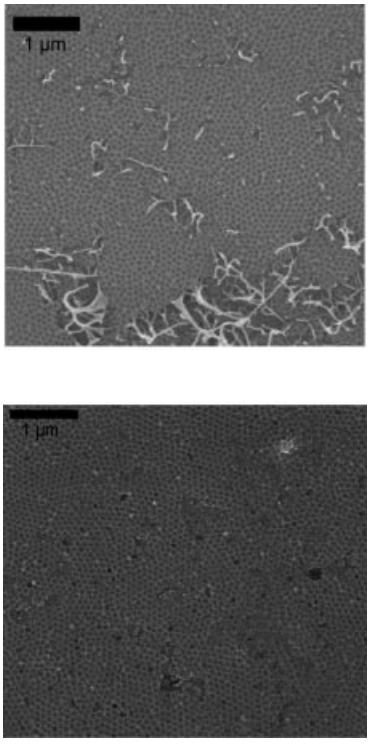

Figure 22. Top: SEM image of a PPX film obtained after deposition on the backside of a PAOX membrane. The fibrous structures result from the destruction of the PAOX film during the mechanical detachment process; bottom: SEM image of a PPX film detached chemically from the PAOX backside by HF dissolution.

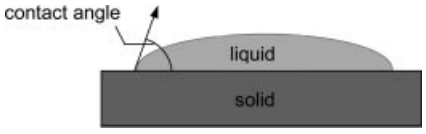

Figure 23. Definition of the contact angle Θ of a liquid on a solid surface.

a flat unstructured PPX film with a contact angle of 86°. This difference of more than 60° is caused by the structuring of the PPX surface with the regular nanopattern. A possible explanation for the reinforcement of the hydrophilicity of the structured PPX relative to the flat PPX surface can be given when considering the model developed by Wenzel, who has theoretically treated liquid wetting of small-scale rough surfaces (Figure 24).[73] A further refined model for superhydrophilic surfaces (superwetting) was developed recently by Quéré.[74]

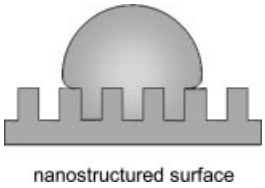

Figure 24. Schematic model of roughness filling of a nanostructured surface by water according to the Wenzel theory.[73]

In the Wenzel model, the space between the protrusions (Figure 24) is filled by a liquid (water), and the theory predicts that both hydrophilicity and hydrophobicity are reinforced by this surface roughness according to the relation:[73]

$\cos\Theta_w = r \cos\Theta_t$

Here Θ_w is the apparent angle on the rough surface (e.g. structured PPX, Figure 22), Θ_t is the contact angle of water on a smooth surface of identical chemical composition (e.g. unstructured PPX film), r is a roughness factor, which is defined as the ratio of the actual surface area over the projected area.

As a result, the contact angle Θ of a surface can be tuned by its surface roughness in the hydrophilic region ($\Theta < 90°$) much in the same way as it can be done in the hydrophobic region ($\Theta > 90°$).[74,75] Thus, a structural change in the surface morphology of the polymeric PPX film is able to tailor the surface wetting of this material from weakly hydrophilic to strongly hydrophilic (Figure 25).

4. Conclusions

Nanoporous alumina is an extraordinary material for synthesis and alignment of nanomaterials. Its straightforward synthetic access, its availability in different sizes and shapes, and most important, its high porosity with a massive number of pores running parallel through the transparent material makes this oxidic structure a unique candidate for nanochemistry.

Consequently a wide variety of materials have been synthesized within the pore system of PAOX over the years in a number of different groups. Its high thermal and structural

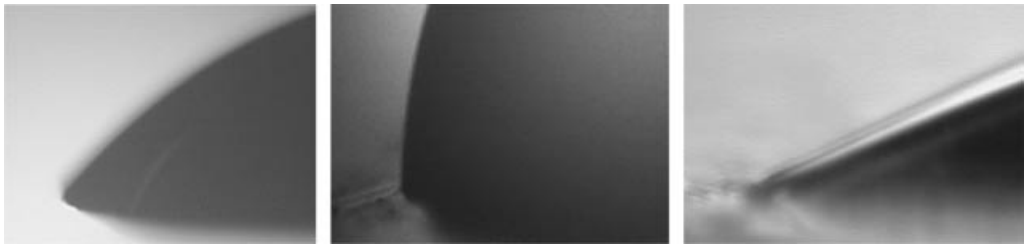

Figure 25. Photographs of the wetting behaviour of water. From left to right: water drop on cleaned glass surface, water drop on flat PPX film surface, water drop on nanostructured PPX film surface (see Figure 22). All contact angles were measured by the sessile drop method.

stability makes PAOX also useful as template in gas-phase CVD processes.

Herein we have described the formation, alignment and FE properties of CNTs inside the pores and on the surface of PAOX. Various single-source precursors were studied and led to the formation of CNTs with and without metal filling of their interior.

In field emission, we found that PAOX has a significant influence on the emission characteristics, which is proven by the highest dc current density so far measured for CNT structures, for example. Moreover long current stabilities of up to 18 h were obtained for these materials after cathode conditioning was employed.

Polymer wires are accessible by a gas-phase route by polymerizing reactive polymer precursors inside the pores of PAOX. Besides the polymerization inside porous alumina, PAOX can be used as a mould to emboss organic polymers. PPX films with a resulting concave surface structure can be deposited on the dome-shaped backside of PAOX and afterwards securely detached from it. This leads to a nanostructured polymer surface, which shows an increased hydrophilicity relative to an unstructured flat PPX polymer film. This may be attributed to an enhanced wetting behaviour of the regular nanopatterned structure relative to a smooth unstructured PPX surface.

The future for even more synthetic as well as technological applications of porous alumina membranes is worth being explored in more detail. Research areas like catalysis, for which its mesopores can be tailored and chemically modified, have been barely touched so far.[76–78] Nanoreactors based on PAOX membranes could be an interesting extension of the already well-established microreactor technique.

Biomolecules are ideal candidates for immobilization inside the pore volume of PAOX because of the variable template pore size in the mesoporous range. Biosensor action is a possible target application that can be realized with such systems.[79] The sector of medical applications of these inorganic membranes is also under current study.[80]

Acknowledgments

Our work was supported by the DFG and the Volkswagenstiftung. The authors gratefully acknowledge the fruitful cooperation in collaborations with FELMI, Graz (EFTEM, Prof. Dr. F. Hofer, TU Graz), with the Erich Schmid Institute of the Austrian Academy of Science, Leoben (Dr. T. Schöberl), both in Austria, and with Prof. Dr. G. Müller, Physics Department, Wuppertal University.

[1] a) M. Terrones, R. Kamalukaran, T. Seeger, M. Rühle, *Chem. Commun.* **2000**, 2335–2336; b) E.-G. Wang, *Adv. Mater.* **1999**, *11*, 1129–1133; c) M. Terrones, P. Redlich, N. Grobert, S. Trasobares, W. K. Hsu, H. Terrones, Y. Q. Zhu, J. P. Hare, C. L. Reeves, A. K. Cheetham, M. Rühle, H. W. Kroto, D. R. M. Walton, *Adv. Mater.* **1999**, *11*, 655–658; d) N. Grobert, M. Terrones, S. Trasobares, K. Kordatos, H. Terrones, J. Olivares, J. P. Zhang, P. Redlicj, W. K. Hsu, C. L. Reeves, D. J. Wallis, Y. Q. Zhu, J. P. Hare, A. J. Pidduck, H. W. Kroto, D. R. M. Walton, *Appl. Phys. A* **2000**, *70*, 175–183.

[2] W. Tremel, *Angew. Chem.* **1999**, *111*, 2311–2315; *Angew. Chem. Int. Ed.* **1999**,*38*, 2175–2179.

[3] a) M. Remskar, Z. Skraba, F. Cleton, R. Sangines, F. Levy, *Appl. Phys. Lett.* **1996**, *69*, 351–353; b) C. M. Zelenski, P. K. Porhout, *J. Am. Chem. Soc.* **1998**, *120*, 734–742; c) L. Margulis, G. Salitra, R. Tenne, M. Taliankar, *Nature* **1993**, *365*, 113–114; d) Y. Feldmann, E. Wassermann, D. J. Srolovitz, R. Tenne, *Science* **1995**, *267*, 222–225.

[4] a) R. L. O. Whitby, W. K. Hsu, C. B. Boothroyd, P. K. Fearon, H. W. Kroto, D. R. M. Walton, *ChemPhysChem* **2001**, *2*, 620–623; b) E. B. Macki, D. H. Galvan, E. Adam, S. Talapatra, G. Yang, A. D. Migone, *Adv. Mater.* **2000**, *12*, 495–498; c) R. Tenne, L. Margulis, M. Genet, G. Hodes, *Nature* **1992**, *360*, 444–446.

[5] a) W. Mickelson, S. Aloni, Wei-Qiang Han, J. Cummings, A. Zettl, *Science* **2003**, *300*, 467–469; b) E. J. M. Hamilton, S. E. Dalton, C. M. Mann, H. O. Cilija, C. A. McDonald, S. G. Shore, *Science* **1993**, *260*, 659–661; c) R. Ma, Y. Bando, T. Sato, K. Kurashima, *Chem. Mater.* **2001**, *13*, 2965–2971.

[6] a) R. B. Wehrspohn, J. Schilling, *MRS Bull.* **2002**, *8*, 263; b) M. S. Sander, A. L. Prieto, R. Gronsky, T. Sands, A. M. Stacy, *Adv. Mater.* **2002**, *14*, 665–667; c) S.-Z. Chu, K. Wada, S. Inoue, M. Isogai, A. Yasumori, *Adv. Mater.* **2005**, *17*, 2115–2119; d) P. P. Mardilovich, A. N. Govyadinov, N. I. Mazurenko, R. Paterson, *J. Membr. Sci.* **1995**, *98*, 143–155; e) N. Itoh, K. Kato, T. Tsuij, M. Hongo, *J. Membr. Sci.* **1996**, *117*, 189–196; f) A. T. Shawaqfeh, R. E. Baltus, *J. Membr. Sci.* **1999**, *157*, 147–158; g) J. H. Yuan, F. Y. He, D. C. Sun, X. H. Xia, *Chem. Mater.* **2004**, *16*, 1841–1844; h) F. Li, L. Zhang, R. Metzger, *Chem. Mater.* **1998**, *10*, 2470–2480; i) A. Michailowski, D. Al-Mawlawi, G. Cheng, M. Moskovits, *Chem. Phys. Lett.* **2001**, *349*, 1–5; j) Y. Wang, J. Y. Lee, H. C. Zjeng, *Chem. Mater.* **2005**, *17*, 3899–3903; k) K. B. Shelimov, M. Moskovits, *Chem. Mater.* **2000**, *12*, 250–254; l) F. Li, J. He, W. L. Zhou, J. B. Wiley, *J. Am. Chem. Soc.* **2003**, *125*, 16166–16167; m) B. A. Hernandez, K. S. Chang, E. R. Fisher, P. K. Dorhout, *Chem. Mater.* **2002**, *14*, 480–482; n) C. Y. Kuo, S. Y. Lu, T.-Y. Wei, *J. Cryst. Growth* **2005**, *285*, 400–407.

[7] G. Schmid, *J. Mater. Chem.* **2002**, *12*, 1231–1238.

[8] T. L. Wade, J.-E. Wegrove, *Eur. Phys. J. Appl. Phys.* **2005**, *29*, 3–22.

[9] F. Keller, M. S. Hunter, D. L. Robinson, *J. Electrochem. Soc.* **1953**, *100*, 411–419.

[10] G. C. Wood, J. P. O'Sullivan, *Proc. R. Soc.* **1970**, *A317*, 511–543.

[11] K. Nielsch, J. Choi, K. Schwirn, R. B. Wehrspohn, U. Gösele, *Nano Lett.* **2002**, *2*, 677–680.

[12] a) S. Ono, N. Masuko, *Corros. Sci.* **1992**, *33*, 503–505; b) S. Ono, H. Ichinose, N. Masuko, *Corros. Sci.* **1992**, *33*, 841–850.

[13] V. P. Parkhuitik, V. I. Shershulsky, *J. Phys.* **1992**, *D25*, 1258–1263.

[14] S. Z. Chu, K. Wada, S. Inoue, S.-I. Todoroki, *Chem. Mater.* **2002**, *14*, 4595–4602.

[15] M. Tian, S. Xu, J. Wang, N. Kumar, E. Wertz, Q. Li, P. M. Campbell, M. H. W. Chan, T. E. Mallouk, *Nano Lett.* **2005**, *5*, 697–703.

[16] H. de L. Lira, R. Paterson, *J. Membr. Sci.* **2002**, *206*, 375–387.

[17] L. J. Gibson, M. F. Ashby, *Cellular Solids: Structure and Properties*, Pergamon Press,**1988**.

[18] a) M. Wada, Y. Kitano, S. Tanase, O. Kajita, T. Sakai, *J. Electrochem. Soc.* **2005**, *152*, A1341–A1346; b) P. T. Kumar, R. Ramesh, Y. Y. Lin, G. T. K. Fey, *Electrochem. Commun.* **2004**, *6*, 520–525.

[19] M. Valcarcel, B. M. Simonet, S. Cardenas, B. Suarez, *Anal. Bioanal. Chem.* **2005**, *382*, 1783–1790.

[20] a) F. Pico, J. M. Rojo, M. L. Sanjuan, A. Anson, A. M. Benito, M. A. Callejas, W. K. Maser, M. T. Martinez, *J. Electrochem. Soc.* **2004**, *151*, A831–837; b) J. H. Chen, W. Z. Li, D. Z. Wang, S. X. Yang, J. G. Wen, Z. F. Ren, *Carbon* **2002**, *40*, 1193–1197;

c) G. Seifert, T. Kohler, T. Frauenheim, *Appl. Phys. Lett.* **2000**, *77*, 1313–1315.
[21] a) S. H. Jeong, H. Y. Hwang, K. H. Lee, Y. Jeong, *Appl. Phys. Lett.* **2001**, *78*, 2052–2054; b) Y. Zhang, J. Liu, X. Li, *Proc. XIV IVMC* **2001**, 13.
[22] a) C. Kocabas, S. H. Hur, A. Gaur, M. A. Meitl, M. Shim, J. A. Rogers, *Small* **2005**, *1*, 1110–1116; b) Z. B. Zhang, J. Cardenas, E. E. B. Campbell, S. L. Zhang, *Appl. Phys. Lett.* **2005**, *87*, 043110/1–043110/3; c) T. Shimada, T. Sugai, Y. Ohno, S. Kishimoto, T. Mizutani, H. Yoshida, T. Okazaki, H. Shinohara, *Appl. Phys. Lett.* **2004**, *84*, 2412–2414.
[23] T. Kyotani, L.-F. Tsai, A. Tomita, *Chem. Mater.* **1996**, *8*, 2109–2113.
[24] T. Yanagishita, M. Sasaki, K. Nishio, H. Masuda, *Adv. Mater.* **2004**, *16*, 429–432.
[25] N. I. Maksimova, J. Engstler, J. J. Schneider, *Nato ASCI Series* **2006**, in press.
[26] J. J. Schneider, N. I. Maksimova, J. Engstler, R. Schierholz, *New. J. Chem.* **2006**, submitted.
[27] P. C. P. Watts, W. K. Hsu, D. P. Randell, V. Kotzeva, G. Z. Chen, *Chem. Mater.* **2002**, *14*, 4505–4508.
[28] H. Hou, A. K. Schaper, F. Weller, A. Greiner, *Chem. Mater.* **2002**, *14*, 3994–3999.
[29] J. J. Schneider, J. Engstler, S. Franzka, K. Hofmann, B. Albert, J. Ensling, P. Gütlich, P. Hildebrandt, S. Döpner, W. Pfleging, B. Günther, G. Müller, *Chem. Eur. J.* **2001**, *7*, 2888–2895.
[30] G. Che, B. B. Lakshmi, E. R. Fisher, C. R. Martin, *Nature* **1998**, *393*, 346–349.
[31] W. Guo, C. Z. Zhu, T. X. Yu, H. Woo, B. Hang, Y. T. Dai, *Phys. Rev. Lett.* **2004**, *93*, 245502/1–245502/4.
[32] H. J. Qi, K. B. K. Teo, K. K. S. Lau, M. C. Boyce, W. I. Milne, J. Robertson, K. K. Gleason, *J. Mech. Phys. Solids* **2003**, *51*, 2213–2237.
[33] Y. R. Jeng, P. C. Tsai, T. H. Fang, *J. Chem. Phys.* **2005**, *122*, 224713/1–224713/8.
[34] C. N. R. Rao, A. Govindaraj, *Acc. Chem. Res.* **2002**, *35*, 998–1007 and references cited therein.
[35] J. Wu, B. E. Hamaoui, J. Li, L. Zhi, U. Kolb, K. Müllen, *Small* **2005**, *1*, 210–212.
[36] L. Zhi, T. Gorelik, R. Friedlein, J. Wu, U. Kolb, W. R. Salaneck, K. Müllen, *Small* **2005**, *1*, 798–801.
[37] See also: a) C. N. R. Rao, B. Satishkumar, A. Govindarai, M. Nath, *ChemPhysChem* **2001**, *2*, 78–105; b) C. N. R. Rao, R. Sen, B. C. Satishkumar, A. Govindarai, *Chem. Commun.* **1998**, 1525; c) C. N. R. Rao, A. Govindaraj, *Acc. Chem. Res.* **2002**, *35*, 998–1007.
[38] a) A. R. Harutyunyan, G. Chen, P. C. Eklund, *Appl. Phys. Lett.* **2003**, *82*, 4794–4796.
[39] A. R. Harutyunyan, G. Chen, P. C. Eklund, *Appl. Phys. Lett.* **2003**, *82*, 4794–4796.
[40] Y. Saito, S. Uemura, *Carbon* **2000**, *38*, 169–182.
[41] a) P. M. Ajayan, O. Stephan, C. Colliex, D. Trauth, *Science* **1994**, *265*; 1212–1214; b) J. I. Sohn, S. Lee, *Mat. Res. Soc., Symp. Proc.* **2001**, *63A*, 14.9.1–14.9.6; c) Y.-H. Lee, Y.-T. Jang, D.-H. Kim, J.-H. Ahn, B. K. Ju, *Adv. Mater.* **2001**, *13*, 479–482; d) X. Xu, G. R. Brandes, *Mat. Res., Symp. Proc.* **1998**, *509*, 107; e) L. A. de Heer, D. Ugarte, A. Chatelain, *Science* **1995**, *270*, 1179–1180.
[42] a) M. J. Fransen, T. L. van Rooy, P. Kruit, *Appl. Surf. Sci.* **1999**, *146*, 312–327; b) J. W. Gadzuk, E. W. Plummer, *Rev. Mod. Phys.* **1973**, *45*, 487.
[43] β is the electrical field enhancement factor of an external electrical field applied to an emitting structure. It is greatly influenced (aside from other factors) by a high aspect ratio of the emitting structure. β is a measure of the lowering of the onset field of FE which is typically between E = 1–10 V μm^{-1} for CNTs. β for MWCNTs can be determined from a Fowler-Nordheim plot assuming a work function of 4.6 eV for graphite.
[44] B. Günther, A. Göhl, G. Müller, J. Engstler, J. J. Schneider, *Proc. 13th IVMC* **2001**, *207*, 2000.
[45] M. Stammler, J. Ristein, T. Habermann, A. Göhl, K. Janoschowsky, D. Nau, G. Müller, L. Ley, *Diam. Relat. Mater.* **1999**, *8*, 792–792.
[46] a) T. Habermann, A. Göhl, D. Nau, M. Wedel, G. Müller, M. Christ, M. Schreck, B. Stritzker, *J. Vac. Sci. Technol.* **1998**, *B16*, 693–696; b) A. Göhl, T. Habermann, G. Müller, D. Nau, M. Wedel, G. Müller, M. Christ, M. Schreck, B. Stritzker, *Diam. Relat. Mater.* **1998**, *7*, 666–670.
[47] a) F. M. Charbonnier, W. A. Mackie, T. Xie, P. R. Davis, *Ultramicroscopy* **1999**, *79*, 73–82; b) S. Kanemaru, T. Hirano, H. Tanoue, J. Itoh, *J. Vac. Sci. Techn.* **1996**, *B14*, 1885–1888; c) M. S. Chung, B.-G. Yoon, J. M. Park, K.-Y. Ha, *Appl. Surf. Sci.* **1999**, *146*, 138–142.
[48] a) N. N. Chubun, A. G. Chakhovskoi, M. Hajra, C. E. Hunt, *J. Vac. Sci. Technol. B* **2003**, *21*, 483–485; b) M. Hajra, N. N. Chubun, A. G. Chakhovskoi, C. E. Hunt, K. Liu, A. Murali, S. H. Risbud, T. Tyler, V. Zhirnov, *J. Vac. Sci. Technol. B* **2003**, *21*, 458–463; c) B. R. Chalamala, R. H. Reuss, K. A. Dean, *Appl. Phys. Lett.* **2001**, *78*, 2375–2377.
[49] J. M. Kim, W. B. Choi, N. S. Lee, J. E. Jung, *Diam. Relat. Mater.* **2000**, *9*, 1184–1189.
[50] O. Gröning, O. M. Küttel, C. Emmenger, P. Gröning, L. Schlappbach, *J. Vac. Sci. Technol.* **2000**, *B18*, 665–678.
[51] L. Nilsson, O. Groenning, C. Emmengger, O. Kuettel, E. Schaller, L. Schlappach, H. Kind, J.-M. Bonard, K. Kern, *Appl. Phys. Lett.* **2000**, *76*, 2071–2073.
[52] J. L. Kwo, M. Yokoyama, W. C. Wang, F. Y. Chuang, I. N. Lin, *Diam. Relat. Mater.* **2000**, *9*, 1270–1274.
[53] S. Kanemaru, T. Hirano, H. Tanoue, J. Itoh, *Appl. Surf. Sci.* **1997**, *111*, 218–223.
[54] J. I. Sohn, S. Lee, Y.-H. Song, S.-Y. Choi, K.-I. Cho, K. S. Nam, *Curr. Appl. Phys.* **2001**, *1*, 61–65.
[55] D. N. Davydov, P. A. Sattari, D. AlMawlawi, A. Osika, T. L. Daslett, M. Moskovits, *J. Appl. Phys.* **1999**, *86*, 3983–3987.
[56] a) J. S. Suh, K. S. Jeong, J. S. Lee, I. Han, *Appl. Phys. Lett.* **2002**, *80*, 2392–2394; b) S. H. Jeong, H. Y. Hwang, K. H. Lee, Y. Jeong, *Appl. Phys. Lett.* **2001**, *78*, 2052–2054; c) Z. H. Yuan, H. Huang, Y. Dang, J. E. Cao, B. H. Hu, S. S. Fan, *Appl. Phys. Lett.* **2001**, *78*, 3127–3129.
[57] F. Kaldasch, B. Günther, G. Müller, J. Engstler, J. J. Schneider, *Proc. IVMC* **2001**, *01TH8586*, 25.
[58] J. Engstler, dissertation University Duisburg-Essen, Essen, **2003**.
[59] D. Lysenkov, H. Abbas, G. Müller, J. Engstler, K. P. Budna, J. J. Schneider, *J. Vac. Sci. Technol. B* **2005**, *23*, 809–813.
[60] B. Günther, dissertation, University Wuppertal, WUB Diss.02-8, **2002**.
[61] H. Masuda, K. Nishio, N. Baba, *Jpn. J. Appl. Phys.* **1992**, *31*, 1775–1777.
[62] H. Masuda, K. Fukuda, *Science* **1995**, *268*, 1466–1468.
[63] C. Goh, K. M. Coakley, M. D. McGehee, *Nano Lett.* **2005**, *5*, 1545–1549.
[64] M. Steinhart, J. H. Wendorff, A. Greiner, R. B. Wehrspon, K. Nielsch, J. Schilling, J. Choi, U. Gösele, *Science* **2002**, *296*, 1997.
[65] A. H. Greiner, J. H. Wendorf, M. Steinhart, *Nachr. Chem.* **2004**, *52*, 426–431.
[66] S. I. Moon, T. J. McCarthy, *Macromolecules* **2003**, *36*, 4253–4255.
[67] H. Xiang, K. Shin, T. Kim, S. I. Moon, T. J. McCarthy, T. P. Rusell, *Macromolecules* **2004**, *37*, 5660–5664.
[68] Ph. Hanefeld, O. Kriha, J. Engstler, M. Steinhart, U. Gösele, J. H. Wendorff, A. Greiner, J. J. Schneider, *Chem. Mater.* **2006**, in press.
[69] W. F. Gorham, *J. Polym. Sci. Part A-1* **1966**, *4*, 3027–3039.
[70] J. Böing, Diss., RWTH Aachen, **2003**.

[71] E. Martines, K. Seunarine, H. Morgan, N. Gadegaard, C. D. W. Wilkinson, M. O. Riehle, *Nano Lett.* **2005**, *5*, 2097–2103.
[72] D. Klee, J. Böing, H. Höcker, *Mater.-wiss. u. Werkstofftech.* **2004**, *35*, 186–191.
[73] R. N. Wenzel, *Ind. Eng. Chem.* **1936**, *28*, 988–994.
[74] D. Quéré, *Phys. A* **2002**, *313*, 32–46.
[75] S. Shibuichi, T. Onda, N. Satoh, K. Tsujii, *J. Phys. Chem.* **1996**, *100*, 19512–19517.
[76] H.-P. Kormann, G. Schmid, K. Pelzer, K. Philippot, B. Chaudret, *Z. Anorg. Allg. Chem.* **2004**, *630*, 1913–1918.
[77] a) D. Höneke, *Appl. Catal.* **1983**, *5*, 179–198; b) D. Höneke, *J. Catal.* **1987**, *105*, 10–18.
[78] D. Höneke, G. Wießmeier, *Ind. Eng. Chem. Res.* **1996**, *35*, 4412–4416.
[79] a) S. Hou, J. Wang, C. R. Martin, *J. Am. Chem. Soc.* **2005**, *127*, 8586–8587; b) P. Kunit, C. R. Martin, *Curr. Pharm. Biotechnol.* **2005**, *6*, 35–467; c) F. Matsumoto, K. Nishio, H. Masuda, *Adv. Mater.* **2004**, *16*, 2105–2108; d) F. Matsumoto, M. Kamiyama, N. Kazuyuki, H. Masuda, *Jpn. J. Appl. Phys. Part 2* **2005**, *44*, L355–L358; e) M. Herrmann, *Chem. Mater.* **2005**, *17*, 4577–4593; f) V. Benoit, A. Steel, M. Torres, Y.-Y. Yu, H. Yang, J. Cooper, *Anal. Chem*. **2001**, *73*, 2412–2420; g) B. J. Cheek, A. B. Steel, M. P. Torres, Y.-Y. Yu, H. Yang, *Anal. Chem*. **2001**, *73*, 5777–578.
[80] a) Patents: DE 1985542i, C2, **2001**; DE 199910188, 4–45, **2001**; DE 19948783 C2, **2001**; b) E. P. Briggs, M. Karlsson, A. R. Walpole, E. Palsgard, P. R. Wilshaw, *J. Mater. Sci. Mater. Med.* **2004**, *15*, 1–9; c) M. Karlsoon, E. Palsgard, P. R. Wilshaw, L. Di Silvio, *Biomaterials* **2003**, *24*, 3039–3046; d) M. Karlsson, A. Johansson, L. Tang, M. Boman, *Microsc. Res. Technol.* **2004**, *63*, 259–265; e) R. van Beuningen, H. van Damme, P. Boeneder, N. Bastiaensen, A. Chan, T. Kievits, *Clin. Chem.* **2001**, *47*, 1931–1933; f) F. Matsumoto, K. Nishio, H. Masuda, *Adv. Mater.* **2004**, *16*, 2105–2107.

Received: December 23, 2005
Published Online: April 3, 2006

